INDERSCIENCE PUBLISHERS
Linking academia, business and industry through research



International Journal of Critical Infrastructures

ISSN online: 1741-8038 - ISSN print: 1475-3219
https://www.inderscience.com/ijcis

Construction of a full lifecycle risk assessment model for high-altitude tension clamps in substations

Bo Sun, Changhao Yu, Lei Cao, Lei Fan, Jiang Lin

DOI: 10.1504/IJCIS.2026.10081734

Article History:

Received:	08 July 2026
Last revised:	27 August 2026
Accepted:	28 August 2026
Published online:	27 October 2026

Copyright © 2026 Inderscience Enterprises Ltd.

Construction of a full lifecycle risk assessment model for high-altitude tension clamps in substations

Bo Sun*

The Electric Power Research Institute of
Guizhou Power Grid Company,
China Southern Power Grid,
Guizhou, Guiyang,
550000, China
Email: bos741@mls.sinanet.com
*Corresponding author

Changhao Yu and Lei Cao

Guizhou Power Grid Company,
China Southern Power Grid,
Guizhou, Guiyang,
550000, China
Email: jiffer026@126.com
Email: kime9267@126.com

Lei Fan

The Electric Power Research Institute of
Guizhou Power Grid Company,
China Southern Power Grid,
Guizhou, Guiyang,
550000, China
Email: hunki762@sina.com

Jiang Lin

Nanjing Deruan Information Technology Development Co., Ltd.,
Jiangsu, Nanjing,
211500, China
Email: pretia087@126.com

Abstract: Tension clamps are vital hardware for mechanical fixation and electrical connection of substation overhead lines, whose failures pose a serious threat to grid operation safety. This paper proposes a full-lifecycle risk assessment model integrating physics-of-failure and data-driven dual prediction. X-DR images of clamps were collected to build a dataset containing five crimping defects, and were processed via Gaussian filtering, CLAHE and Gamma correction; object detection algorithms realise automatic defect identification and positioning. Lifecycle risk factors covering design, manufacturing, installation, operation-maintenance and retirement are extracted

Copyright © The Author(s) 2026. Published by Inderscience Publishers Ltd. This is an Open Access Article distributed under the CC BY license. (http://creativecommons.org/licenses/by/4.0/)

with factor-failure mechanism mappings. A four-dimensional risk index system was weighted by the AHP-entropy method, and a quantitative risk model with four-tier criteria was established to evaluate failure probability and associated losses. Case studies using regional grid X-DR data verify its performance in defect detection and risk quantification, supporting condition-based maintenance and full-lifecycle decision-making for tension clamps.

Keywords: tension clamp; full lifecycle; risk assessment; X-DR detection; thermal breakdown.

Reference to this paper should be made as follows: Sun, B., Yu, C., Cao, L., Fan, L. and Lin, J. (2026) 'Construction of a full lifecycle risk assessment model for high-altitude tension clamps in substations', *Int. J. Critical Infrastructures*, Vol. 22, No. 15, pp.1–29.

Biographical notes: Bo Sun received his Master's degree in Control Engineering from Northeast Electric Power University in 2019. He is currently an Engineer at the Electric Power Research Institute of Guizhou Power Grid Company, China Southern Power Grid. His research interests include non-destructive testing and failure analysis of primary equipment in substations, failure analysis of power grid materials, as well as technical management of grid primary equipment.

Changhao Yu is a senior engineer with a Master's degree working at China Southern Power Grid Guizhou Power Grid Corporation. His research focuses on condition maintenance of high-voltage substation equipment, intelligent substation operation and maintenance, and full-life-cycle technical supervision for substation specialties. He has rich engineering experience in substation equipment management and technical supervision. Has long spearheaded the remediation of substation hazards, equipment technical upgrades, and the implementation of digital inspection technologies.

Lei Cao is a Senior Engineer with a Master's degree at China Southern Power Grid Guizhou Power Grid Corporation. His research focuses on intelligent substation operation and maintenance and full-process technical management of substation projects. He has accumulated abundant practical experience in substation construction management and intelligent operation technical support, and participates in multiple grid technical research works. He has long led the O&M of secondary systems for smart substations and the tiered management and control system for existing substation equipment.

Lei Fan is a Senior Engineer with a Master's degree at the Electric Power Research Institute of China Southern Power Grid Guizhou Power Grid Corporation. His research covers new energy storage technologies and power grid material failure analysis. He takes part in multiple grid research projects and combines theoretical analysis with laboratory tests to solve material failure and energy storage application problems.

Jiang Lin holds a Master's degree and works as a Senior Electrical Engineer at Nanjing Deruan Information Technology Development Co., Ltd. His research mainly involves novel power system construction, online condition monitoring and intelligent fault diagnosis of various power equipment. He has long been devoted to related power technology theoretical research and practical engineering development projects.

1 Introduction

Tension clamp is a key piece of hardware for achieving mechanical fixation and electrical connection of wires in overhead lines of substations (Du et al., 2025), widely used in critical locations such as incoming and outgoing line structures, busbar sections, and equipment down conductors. Its operational reliability is directly related to the safe and stable operation of substations and even regional power grids (Liu et al., 2025). In recent years, with the continuous expansion of the power grid scale and the increasingly prominent problem of aging equipment (Wu et al., 2025a), line faults caused by the failure of tension clamps have occurred from time to time. Statistics show that a considerable proportion of unplanned shutdowns of overhead lines are caused by overheating or breakage of clamp type fittings (Sun et al., 2024), with poor crimping quality during installation and increased contact resistance during operation being the main causes. Therefore, conducting a full life cycle risk assessment of tension clamps (Shen et al., 2026) is of great significance for improving the reliability of power grid operation by enabling a shift from 'post-maintenance' to 'pre-warning'.

Zhou et al. (2025) proposed a new risk assessment method based on equipment condition, which utilises quantile mapping techniques to combine trend information from statistical fault data with specific condition information from equipment condition monitoring data. Firstly, construct an equipment fault model based on statistical fault data; subsequently, the quantile mapping technique was used to incorporate equipment condition data into the fault model, thereby achieving more accurate risk assessment; finally, maintenance costs are determined based on the risk assessment results. However, this method highly relies on the completeness and quality of statistical fault data. If historical fault data is insufficient or incomplete, the accuracy of quantile mapping will be significantly affected, particularly when applied to hidden crimping defects that occur during installation. The lack of corresponding prior knowledge in the statistical fault distribution leads to a regression of the mapping results to the mean, making it difficult to identify the differentiated risks of individual devices. The purpose of Sun et al. (2023) substation risk assessment is to provide a series of risk quantification indicators, which comprehensively reflect the operation status of the substation and the consequences of accidents from multiple temporal and spatial dimensions. As an important component of the substation network, the failure of substation equipment is one of the fundamental causes of system accidents. This method focuses on the macro risk situation assessment at the substation level, using equipment failures as input conditions to analyse system consequences. However, it does not delve into the micro degradation process of individual equipment from health status to failure, and lacks explicit modeling capabilities for continuous degradation processes such as the gradual increase in contact resistance of tension clamps and the critical transition of thermal breakdown. For single metal fittings such as tension clamps, which are relatively simple in structure and have clear failure mechanisms, their risks mainly depend on the degradation of their physical state. Nicolae et al. (2023) quantitatively determines risk/safety levels. For key power infrastructure such as high-voltage substations, the role of occupational health and safety is to ensure the supply of electricity to the national economy, maintain the safety and stability of the working environment, protect the safety of workers and their workplaces, and ensure the stability of industrial and power production processes, thereby achieving the best operation of the national economy and ensuring energy security. This method

focuses on the occupational health and safety risks of substation operators, quantitatively evaluating the level of threat to personal safety in the operation and maintenance scenarios of high-voltage substations. It is constructed around dimensions such as safety protection, operating standards, and working environment, and does not have a corresponding indicator mapping relationship with equipment physical risks such as electrical resistance degradation, thermal breakdown failure, and mechanical strength attenuation of tension clamps. It belongs to different risk categories. Tang et al. (2023) is a comprehensive power flow calculation based on adaptive Levenberg Marquard and Newton methods, which can be used to evaluate the risks caused by overload/overload and voltage deviation. In addition, graphics processing units are also used for parallel processing of computationally intensive tasks. The numerical experimental results show that the proposed I-ORA algorithm can accurately assess the risks of the entire integrated transmission and distribution network, and its efficiency and convergence are quite good. This indicates that the algorithm will help improve the coordinated operation level of the integrated transmission and distribution network in the future. This method is essentially an operational risk assessment tool for power grid flow safety, and its risk sources are concentrated on the power quality and power transmission capacity on the grid side, rather than the physical health status of the equipment itself, making it difficult to directly transfer to individual health risk prediction of hardware components.

In summary, the existing risk assessment methods have the following main bottlenecks when targeting individuals with tension clamps:

1 Macro system level assessment methods lack the ability to finely characterise the physical process of single hardware failure, making it difficult to establish a complete causal chain from material degradation, contact interface degradation to functional failure.

2 The statistical driven method lacks prior fault data support for hidden defects (such as crimping leakage, bending, flying edges, etc.) that occur during the installation phase, resulting in systematic underestimation of such high-risk initial defects in the evaluation.

3 The evaluation index system for personal safety or power grid flow lacks a corresponding mapping relationship with the physical risks of the equipment itself, and cannot be directly used for the health status evaluation of hardware components. The root cause of the above bottleneck lies in the failure of existing methods to effectively integrate the physical mechanisms of failure with data-driven prediction, in order to simultaneously address the dual challenges of clear mechanisms but difficult parameter acquisition, and rich data but imbalanced samples.

In response to the above issues, this article proposes a full lifecycle risk assessment model for high-altitude tension clamps in substations. The overall construction idea of this model follows a progressive technical route of ‘state perception → indicator quantification → probability prediction → risk grading’:

Firstly, using X-DR image intelligent detection as the data entry point, combined with the division of the entire lifecycle stages, the system identifies key risk factors in each stage of design, manufacturing, installation and operation, operation and maintenance, and retirement and scrapping.

Secondly, a risk assessment index system is constructed from four dimensions: technology, environment, operation, and detection, and the AHP entropy method is used to combine weighting to achieve standardised quantification of multi-source indicators.

Then, the core method of this article is constructed – a dual track fusion prediction model based on 'thermal breakdown physical mechanism driven' and 'A-DBiLSTM data feature driven', to dynamically evaluate and cross validate the probability of clamp failure.

Finally, the fused failure probability is combined with the failure consequences to develop a four level risk classification standard.

The core and novel contributions of this paper compared with the existing most advanced methods are reflected in the following three aspects: first, in terms of prediction methods, life prediction driven by thermal breakdown physical mechanism and state degradation prediction driven by A-DBiLSTM data are included in the unified dual track fusion framework for the first time, and a dynamic weight distribution mechanism based on prediction confidence is introduced, so that the fusion results have both physical consistency and data adaptability, breaking the inherent limitations of a single model in generalisation ability or interpretability; secondly, a four-dimensional evaluation system consisting of technology environment operation detection was established in the indicator system, and the severity score of installation defects obtained from X-DR image detection was included as the initial health baseline as the evaluation input, achieving closed-loop connectivity of risk factors across the entire time scale; thirdly, in engineering applications, the defined comprehensive risk value $R(t)$ is directly linked to the four level risk level for differentiated operation and maintenance strategies, establishing an end-to-end link from probability output to executable decisions, filling the gap in existing methods for fine risk assessment of individual hardware fittings.

2 Identification of risk factors and state perception throughout the entire lifecycle

The comprehensive identification of risk factors throughout the entire lifecycle and effective acquisition of state perception data are prerequisites and physical foundations for conducting subsequent quantitative assessments and risk predictions. This chapter serves as the 'data and perception layer' of the evaluation model, aiming to address the questions of 'what are the sources of risk' and 'where do state data come from', firstly, introduce the structural characteristics of tension clamps (Wu et al., 2025b); subsequently, the construction method of X-DR image dataset is elaborated, including on-site acquisition process, defect classification and annotation, and image pre-processing techniques; finally, from the perspective of the entire lifecycle, the key risk factors at each stage are summarised, laying a theoretical and data foundation for the construction of the subsequent risk assessment index system (Chen and Xu, 2026).

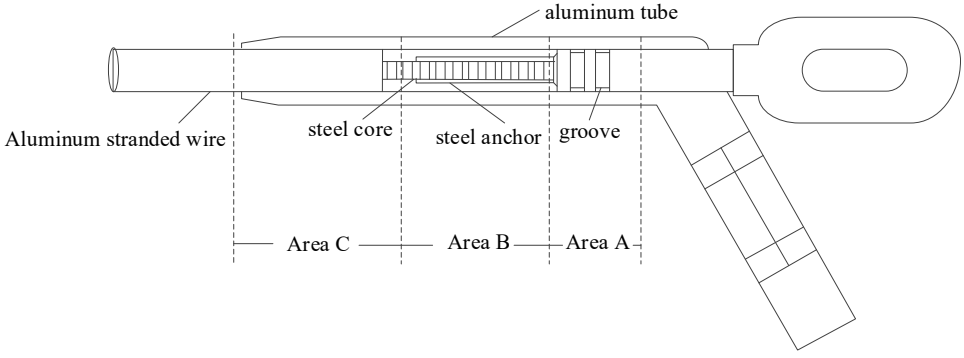
2.1 Construction and pre-processing of tension clamp X-DR image dataset

Tension clamps are essential hardware components in overhead power lines of substations, mainly used to withstand wire tension and secure wires to insulator strings of tension towers or substation structures (Baghmisheh et al., 2023). In the substation

scenario, tension clamps are usually installed at key positions such as incoming and outgoing line structures, busbar sections, and equipment down conductors, serving the dual functions of mechanical fixation and electrical connection of wires. The structural reliability directly affects the safe and stable operation of overhead power lines in substations.

For the commonly used steel core aluminium stranded wire tension clamps for overhead transmission lines, the crimping positions mainly include zone A (where the steel anchor groove connects to the aluminium tube), zone B (where the steel anchor connects to the steel core), and zone C (where the aluminium stranded wire connects to the aluminium tube). When non-destructive testing is carried out using X-DR technology, the above three areas are the key testing locations (Mao et al., 2025). The compression structure of the tension wire clamp is shown in Figure 1.

Figure 1 Compression structure of tension wire clamp



The centre of the X-ray beam should be directed vertically towards the line clamp to be tested, and the imaging board should be kept tightly attached to the clamp; if the on-site conditions are limited and cannot maintain close contact, the focal length should be appropriately increased. At the same time, the testing personnel must always remain on the other side of the radiation source to avoid exposure to the radiation range (Shi et al., 2025).

The imaging focal length of the radiation generating device should meet the following requirements:

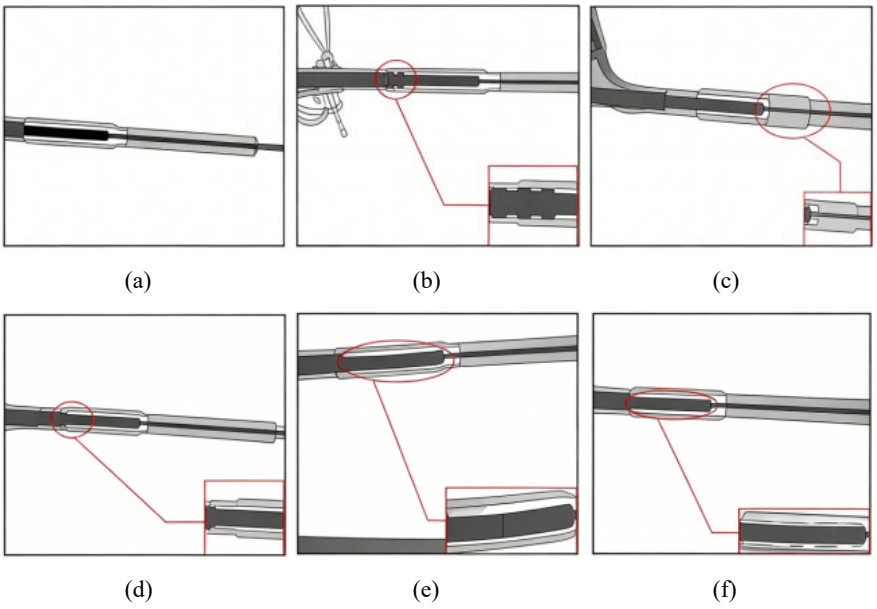
$$F \geq (d+1) \cdot f_2 \tag{1}$$

In the formula, F is the imaging focal length, d is the camera focal diameter (Liu et al., 2024b), and f_2 is the detector pixel size. The crimping defects are divided into five categories: A-zone leakage, C-zone leakage, overvoltage, bending, and flash. The typical X-DR image features are described in Figure 2.

The definitions and hazard characteristics of various types of defects are as follows:

- Firstly, leakage of pressure in zone A: The aluminium tube and steel anchor groove are not crimped or crimped incompletely, leaving a gap between the two. This type of defect directly endangers the tensile strength of the wire clamp (Wang et al., 2024), and belongs to the highest hazard level defect type. Once discovered, the heavy pressure should be promptly disconnected.

Figure 2 Schematic diagram of tension clamp defects, (a) defect-free (b) pressure loss in area A (c) leakage pressure in zone C (d) overvoltage (e) bend (f) flash (see online version for colours)



- Secondly, leakage voltage in zone C: Incomplete or not crimped in zone C, this defect significantly increases the contact resistance while reducing the tension performance of the wire clamp, and increases the Joule heat loss and temperature rise risk of the circuit.
- Thirdly, overvoltage: Excessive crimping can cause compression in the non-compression zone, which may lead to cracking or deformation in the non-compression zone, affecting the structural integrity and tensile strength of the wire clamp (Liu et al., 2024a).
- Fourth, bending: The surface of the steel anchor undergoes deformation and bending due to external forces, which affects the uniformity of the force on the clamp and the accuracy of the crimping fit.
- Fifth, flying edge: The protrusions or burrs on the surface of the steel anchor may become a source of stress concentration and induce crack initiation under dynamic loading.

Pre-processing of tension clamp X-DR images is required (Lin and Xu, 2023). The image pre-processing method used in this article is divided into two steps: image expansion and image enhancement.

2.1.1 Data expansion

A single X-DR image may contain multiple types of crimping defects, and the same type of defect may appear in multiple places. If the entire image is directly processed to expand the number of defects, it is difficult to effectively alleviate the problem of

imbalanced samples in the dataset. Therefore, this article adopts the strategy of 'cutting first, then expanding' (Zhang et al., 2024), with the following specific steps:

Step 1 Take the images in the dataset containing defects such as 'C-zone leakage pressure', 'bending', and 'flying edge' as input, and proceed directly to step 2 for the remaining images.

Step 2 Establish an image coordinate system based on the length and width of the input image, read the position coordinates of each target defect in the label file, locate and crop them, and obtain a single target defect image.

Step 3 Scale, flip, and mirror the cropped images at random angles to construct a single target defect image dataset, and re label the augmented images (Yan et al., 2023) to expand the dataset.

2.1.2 Image enhancement

The tension clamp X-DR image is easily affected by factors such as the voltage of the radiation tube, the number of pulses, and the insensitivity of the imaging equipment's photosensitive components, resulting in unclear features in the crimping area. To this end, this article uses three methods in sequence: Gaussian filtering, constrained contrast histogram equalisation (CLAHE), and Gamma correction to enhance the contrast of the dataset, in order to improve the clarity of image features and enhance the accuracy of defect detection.

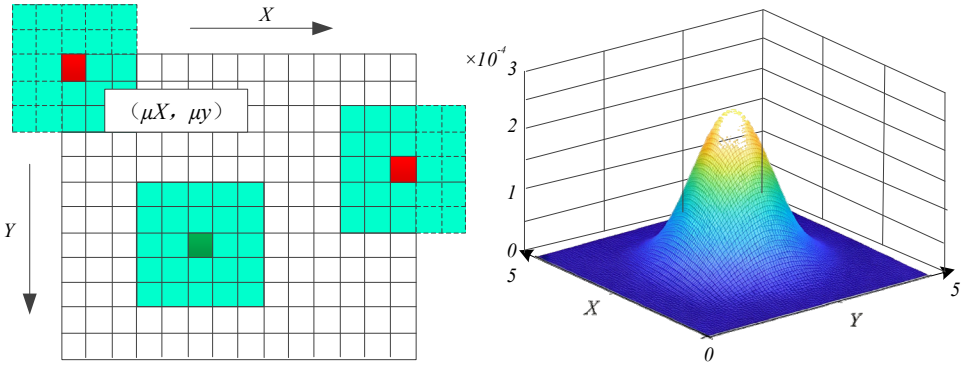
1 Gaussian filtering: The noise present in the image can interfere with the effective transmission of information and affect the training performance in deep learning. This article uses Gaussian filtering to denoise X-DR images. This method is based on constructing filters using Gaussian functions, which smooth the image and eliminate noise by performing convolution operations on the image. Take the neighbourhood of each pixel in the image as a rectangular window, and perform a weighted average of the pixel values of all pixels within the window. The weights follow a two-dimensional normal distribution, and weight $H(x, y)$ is represented as follows:

$$H(x, y) = \frac{1}{\left(\sqrt{2\pi\sigma^2}\right)} e^{\frac{-\left[(x-\mu_x)^2+(y+\mu_y)^2\right]}{2\sigma^2}} \tag{2}$$

In the formula, σ is the standard deviation, (x, y) is the coordinate of any point within the rectangular window, and μ_x, μ_y is the centre coordinate of the rectangular window. This article takes $\sigma = 2$ and the rectangular window is 5 × 5. The pixels in the original image are denoted as $f(x, y)$. After passing through the filtering window pixel by pixel, the filtered image pixels can be represented as $g(x, y) = f(x, y) \times H(x, y)$. After Gaussian filtering, the noise in the image is effectively suppressed, the overall clarity is improved, and the detail information is also enhanced.

This article takes $\sigma = 2$ and a rectangular window of 5 × 5 as an example to draw its weight distribution as shown in Figure 3. It can be seen that the weights closer to the centre of the rectangular window (2.5, 2.5) are larger.

Figure 3 Schematic diagram of Gaussian filtering principle, (a) Gaussian filtering process (b) the three-dimensional distribution of weights (see online version for colours)



(a) (b)

2 Limit contrast histogram equalisation (CLAHE): Restricted contrast histogram equalisation (CLAHE) introduces restriction operations on the basis of traditional methods, which can effectively avoid the above problems.

This article uses CLAHE to enhance the contrast between target defects and background in X-DR images. The specific steps are as follows: firstly, the image is segmented into local blocks of $L \times L$, and assuming that the number of pixels in each local block is M, the histogram of each local block is calculated. The histogram distribution probability $P_r(r_k)$ of the original image is:

$$P_r(r_k) = \frac{n_k}{n} (0 \le r_k \le 1, k = 0, 1, \ldots, l-1) \tag{3}$$

In the formula, r_k is the k^{th} grey level, n_k is its corresponding number of pixels, n is the total number of image pixels, and k is the current accumulated grey level number. Subsequently, the histogram cumulative distribution function S_k is used to correct the image grey level:

$$S_k = T(r_k) = \sum_{j=1}^{k} \frac{n_j}{n} = \sum_{j=1}^{k} p_r(r_j) (0 \le r_j \le 1) \tag{4}$$

In the formula, r_j is the j^{th} grey level, $p_r(r_j)$ is the probability density of the j^{th} grey level, and S_k is the cumulative distribution function.

Secondly, calculate the shear threshold β for each local block, which can control the degree of contrast gain. The specific calculation method can be expressed as:

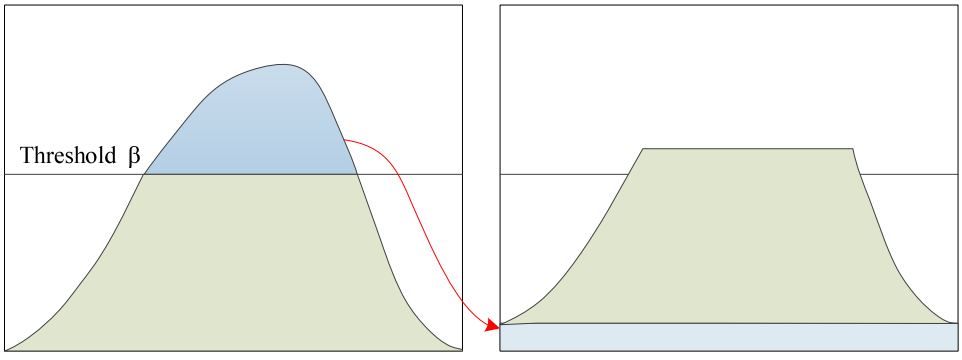
$$\beta = \frac{N}{M} + \frac{(N - N/M)}{\alpha} \tag{5}$$

In the formula, α is the contrast enhancement amplitude limiting coefficient, and N is the number of pixels after histogram equalisation in each region. Apply the cropping threshold to the histogram of each local block in the original image for cropping. The parts with pixel greyscale values higher than the cropping threshold will be evenly

distributed to the low greyscale areas of the image, as shown in Figure 4. The calculation method for the number of pixels ξ added to the low greyscale areas is as follows:

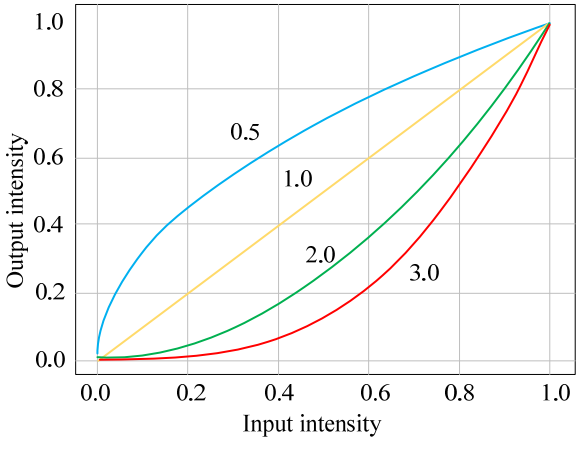
$$\xi = \sum_{x=0}^{M-1} \max\left\{\left[T(r_k) - \beta\right], 0\right\} \Big/ M \tag{6}$$

Figure 4 Schematic diagram of CLAHE cutting (see online version for colours)



3 Gamma correction: The contrast enhancement algorithm may result in excessive enhancement or unclear enhancement effect. In this paper, Gamma correction is further used for nonlinear tone editing as shown in Figure 5.

Figure 5 Gamma curve (see online version for colours)



For any pixel in the original image, first normalise it to the 0–1 interval, then $1/\gamma$ is calculate the pre compensation value for the index, and finally denormalise it to an integer value in the 0–255 interval. When $\gamma < 1$, the dynamic range of low greyscale areas in the image expands and the overall brightness increases; When $\gamma > 1$, the dynamic range of the high greyscale area expands and the overall brightness decreases. By adjusting the index, the image contrast can be flexibly adjusted.

This article sequentially applies Gaussian filtering, CLAHE, and Gamma correction to the tension clamp X-DR images. The processed images show significant improvements in clarity and contrast at the crimping site, providing a high-quality image data foundation for subsequent defect automatic recognition based on deep learning. On the basis of completing image pre-processing, an object detection algorithm is used to automatically identify and locate five types of crimping defects in the tension clamp X-DR image. The current mainstream single-stage object detection models (such as YOLO series) have been widely used in DR image defect detection of power equipment due to their fast detection speed and high accuracy.

The core of object detection lies in extracting image features through convolutional neural networks, predicting the category and bounding box position of defective targets. For the input image, the model divides it into grid cells of $S \times S$, and each grid is responsible for predicting whether there are defective targets and their location information within its region. The predicted bounding box is parameterised using centre coordinates (x, y), width w, height h, and confidence score c.

The loss function during model training consists of three parts: bounding box position loss L_{loc}, confidence loss L_{conf}, and category loss L_{cls}:

$$L = \lambda_{loc} L_{loc} + \lambda_{conf} L_{conf} + \lambda_{cls} L_{cls} \tag{7}$$

Among them, λ_{loc}, λ_{conf}, and λ_{cls} are the weight coefficients corresponding to each loss item, used to balance the impact of each loss item on the total loss; position loss L_{loc} is usually measured using intersection over union (loU) and its derived indicators. LOU is defined as the intersection $IoU = \dfrac{|B_p \cap B_g|}{|B_p \cup B_g|}$ between predicted box B_p and real box B_g. The closer the IoU value is to 1, the more accurate the predicted box positioning is.

To improve the recognition ability of the model for small defects, an efficient channel attention (ECA) mechanism can be introduced in the backbone network. The size of its convolution kernel k and the number of channels C satisfy:

$$k = \psi(C) = \left| \frac{\log_2(C)}{\gamma} + \frac{b}{\gamma} \right| \tag{8}$$

In the formula, γ and b are hyperparameters, with $\gamma = 2$ and $b = 1$; C is the number of channels in the input feature map. This mechanism can effectively highlight the key information of defect feature maps and suppress the interference of non-defect backgrounds.

Through the above method, five types of defects: leakage pressure in zone A, leakage pressure in zone C, overvoltage, bending, and flash can be automatically detected and identified from X-DR images. The detection results can be directly mapped to construction quality defects during the installation and operation stage, providing data support for identifying risk factors throughout the entire lifecycle.

Taking the typical defects revealed by the defect detection results of the image dataset during the installation phase as the starting point, and further combining the

risk characteristics of each stage of the entire lifecycle, the key risk factors of tension clamps are systematically identified from four dimensions: design and manufacturing, installation and operation, operation and maintenance, and retirement and scrapping, laying the foundation for the construction of the subsequent lifecycle risk assessment index system.

2.2 Classification of risk factors and stage mapping throughout the entire lifecycle

Based on the typical defects revealed during the installation phase by X-DR image defect detection in Subsection 2.1, this section further conducts a systematic identification of risk factors throughout the entire lifecycle from a temporal perspective. The research objective of this section is to establish a systematic risk factor classification system for the entire process from design and manufacturing to retirement and scrapping of tension clamps, clarify the typical characteristics of risk factors in each stage and their cross stage transmission laws, and provide a structured factor pool and stage mapping relationship for the construction of the risk assessment index system in Section 3. The core technical obstacles that need to be overcome to achieve this goal include:

1 The significant differences in the manifestation of risk factors in each stage – the material margin in the design stage belongs to the category of design parameters, the crimping defects in the installation stage are manifested as geometric anomalies, and the environmental corrosion and thermal aging in the operation stage are continuous and gradual processes. How to unify the above heterogeneous factors into the same evaluation framework is the primary challenge.

2 The risk transmission between stages has nonlinear and cumulative amplification effects. Hidden defects in the installation stage gradually deteriorate under the effect of electric thermal coupling during operation, and their evolution path is modulated by both load history and environmental conditions, making it difficult to describe with a simple linear superposition model.

3 The quantitative data sources for risk factors in each stage are different – design parameters come from equipment ledgers and factory test reports, construction defects come from X-DR image detection, operational status comes from online monitoring and inspection records, and there is no unified standard for spatiotemporal alignment and fusion of multi-source heterogeneous data.

In response to the above challenges, the solution adopted in this article is as follows: firstly, establish a causal mapping between risk factors and failure modes at each stage based on failure physics, and unify heterogeneous factors into “the degree of influence on three types of underlying physical quantities: contact resistance, mechanical strength, and corrosion margin”; secondly, introducing chain transfer factors to characterise the cumulative and amplification effects of risks at each stage; finally, using the ‘risk transmission chain’ as a unified analytical thread throughout the entire lifecycle, dispersed stage risks are summarised into a causal chain from initial defect implantation to final failure output, in order to avoid the difficulty of direct fusion of heterogeneous data from multiple sources. At the same time, according to the life cycle stages of tension clamps, the risk factors are summarised and analysed throughout the entire process from design and manufacturing, installation and operation, maintenance to retirement and

scrapping, and a mapping relationship between risk factors and the aforementioned failure mechanisms is established.

2.2.1 Design and manufacturing stage

The risk factors in the design and manufacturing stage mainly involve three aspects: material selection, structural design, and processing technology.

In terms of material selection, the choice of material grades for aluminium tubes and steel anchors, as well as the thickness and uniformity of the galvanised layer, directly affect the corrosion resistance and heat resistance of the wire clamp. If the environmental corrosion level or load characteristics of the installation area are not fully considered during the design phase, it may lead to insufficient corrosion resistance or current carrying capacity of the wire clamp, which may pose hidden dangers for subsequent operation.

In terms of structural design, the geometric parameters of the crimping area (such as crimping length and compression ratio) determine the distribution of contact stress and mechanical retention force after crimping. Improper design may lead to insufficient contact pressure or stress concentration after crimping, thereby accelerating the performance degradation of the contact interface during operation.

In terms of processing technology, the annealing treatment process of aluminium tubes, the heat treatment process of steel anchors, and the processing accuracy of crimping moulds all directly affect the quality consistency of the final product. Dimensional deviations during the manufacturing process that exceed the allowable range will result in a decrease in fitting accuracy during on-site crimping, increasing the probability of construction defects.

2.2.2 Installation and operation stage

The risk factors during the installation and operation phase are mainly construction quality defects, which are the main source of early failure. According to the defect classification in Subsection 2.3.2, five types of defects including leakage pressure in area A, leakage pressure in area C, overvoltage, bending, and flash edge are all formed at this stage. The causes and risk characteristics of various defects are as follows:

1 Leakage pressure in zones A and C: Mainly due to non-standard crimping operations, such as insufficient crimping channels, low crimping pressure, or improper selection of crimping moulds, resulting in ineffective crimping between aluminium tubes and steel anchors or aluminium stranded wires. The leakage of pressure in zone A directly endangers the tensile strength of the wire clamp and belongs to the highest risk level defect; the leakage voltage in zone C leads to a significant increase in contact resistance, becoming a hidden source of heat generation faults during operation.

2 Overpressure: Caused by excessive crimping pressure or mismatched mould specifications, resulting in excessive deformation in the non-pressure zone. Overvoltage may induce the initiation of non-pressure zone cracks, which gradually propagate under high-frequency vibration conditions, ultimately leading to the failure of the wire clamp structure.

3 Bending: It is caused by positioning deviation during the crimping process or improper external force during the installation of the wire clamp, resulting in deformation and bending of the steel anchor surface, which affects the uniformity of force distribution at the crimping interface.

4 Flying edge: Due to the wear of the crimping mould or improper setting of crimping parameters, the protrusions or burrs generated on the surface of the steel anchor may become the source of local overheating or stress concentration during operation.

If the above-mentioned construction defects are not investigated by non-destructive testing methods such as X-DR before commissioning, they will enter the operation stage as hidden initial defects and gradually evolve into various failure modes under the long-term effects of current thermal effects and environmental loads. The risk factors during the installation phase also include operational issues such as inadequate tightening torque of hardware connection bolts and weak connection between drainage wires and clamps. These issues also have the characteristics of strong concealment and difficult troubleshooting.

2.2.3 Operation and maintenance phase

The risk factors during the operation and maintenance phase involve three aspects: environmental erosion, load conditions, and detection and maintenance.

1 Environmental erosion factors: The corrosion rate of wire clamps is affected by factors such as salt spray concentration, atmospheric humidity, industrial pollution (such as corrosive gases such as sulphides and nitrogen oxides), and temperature changes. The corrosion risk of tension clamps in coastal or industrial substations is significantly higher than that in inland clean areas. Environmental factors accelerate the electrochemical corrosion of the contact interface, gradually increasing the contact resistance and inducing abnormal temperature rise and thermal breakdown risk. In addition, the thermal expansion and contraction effects caused by the temperature difference between day and night and the seasonal temperature difference may lead to periodic relaxation of the contact pressure at the crimping interface, accelerating the degradation of contact performance.

2 Load condition factors: Long-term heavy load operation (approaching the upper limit of the wire current carrying capacity) exacerbates the Joule heating accumulation effect of the wire clamp and accelerates the thermal aging process. Short circuit current surge, especially in the vicinity of short-circuit faults, may cause the wire clamp to withstand currents several times higher than the rated value for a short period of time, resulting in severe thermal shock and electrodynamic effects. Thermal shock may cause plastic deformation and contact pressure relaxation at the crimping interface, while electrodynamic force may cause mechanical impact on the wire clamp. The coupling effect of the two may cause irreversible damage to the crimping interface.

3 Detecting and maintaining factors: The rationality of operation and maintenance strategies directly affects the controllability of risks. An excessively long infrared temperature measurement cycle may delay the detection of abnormal temperature rise; insufficient coverage of X-DR detection may result in hidden defects not being

identified for a long time. In addition, the lack of systematic accumulation and analysis of detection data constrains the accuracy of state assessment and remaining life prediction.

2.2.4 Retirement and scrapping stage

The risk factors in the retirement and scrapping stage mainly involve the scientificity of the criteria for determining the expiration of the service life and the rationality of retirement decisions. The current retirement judgment of tension clamps is mainly based on empirical regulations of operating years (usually 20–30 years), lacking refined judgment basis based on actual health status. Premature replacement leads to resource waste and increases operation and maintenance costs; late replacement may face the risk of sudden failure, resulting in unplanned power outages.

In addition, the analysis of failure cases of retired clamps is an important data source for improving risk identification and life prediction models. Dissection inspection, metallographic analysis, and mechanical performance testing of retired wire clamps can reveal the laws of material performance degradation and defect evolution during long-term service, but there is still insufficient systematic accumulation in this area.

2.2.5 Phase mapping and correlation analysis of risk factors

The risk factors at each stage have been identified in the previous text, but they must act on the underlying failure mechanism through specific physical/chemical processes in order to ultimately evolve into faults. The core task of this section is to elucidate the specific pathways through which key risk factors trigger or accelerate the three dominant mechanisms of increased contact resistance, mechanical strength degradation, and corrosion failure.

1 The driving mechanism of increasing contact resistance: The gradual increase in contact resistance is the physical root cause of thermal breakdown failure. Risk factors at different stages affect the process through differentiated pathways:

   During the installation phase, the leakage pressure in zone C directly resulted in the effective contact area between the aluminium tube and the aluminium stranded wire being much smaller than the design value. According to the theory of contraction resistance, the contact resistance R_c is approximately inversely proportional to the number of effective contact points n, and the leakage voltage causes the initial contact resistance to be several times higher than the normal value by an order of magnitude. As a surface micro protrusion, the tip effect of the flying edge causes electric field distortion, becoming a ‘hot spot’ where Joule heating preferentially concentrates, accelerating local oxidation and micro ablation, and significantly increasing the time-varying growth rate k of contact resistance compared to the normal region.

   During the operation phase, corrosive gases infiltrate into the micro gaps of the crimping interface to form oxide films or corrosion products, directly increasing the cross-sectional potential barrier and occupying the effective contact channel, causing n to continuously decrease over time. At the same time, the thermal expansion and contraction caused by load fluctuations lead to micrometer level relative slip at the

crimping interface, continuously grinding away benign contact spots and exposing fresh metal surfaces. The latter rapidly oxidises, forming a positive feedback loop of 'wear oxidation re wear', which accelerates the nonlinear growth of contact resistance.

2 The synergistic mechanism of mechanical strength degradation: Mechanical strength failure is a common result of stress concentration on material toughness degradation. During the installation phase, leakage pressure in zone A directly damages the mechanical connection between the steel anchor and the steel core, resulting in a loss of over 50% of the rated tensile strength, which is considered a direct structural failure. Overpressure is equivalent to introducing a cold work hardening layer and microcracks in the flying pressure zone, which significantly reduces the fracture toughness KIC in this area and can greatly shorten the fatigue life. Bending causes an initial deviation angle between the steel anchor axis and the direction of force, introducing additional bending stress in the clamped vibration environment and accelerating the initiation and propagation of fatigue cracks.

3 Chain transmission and multi field coupling effect: The most critical feature of full lifecycle risk is the nonlinear chain transmission – upstream small initial defects are amplified step by step under the action of multiple physical fields during operation. The typical path includes:

- leakage voltage in zone C during installation → high initial contact resistance → abnormal increase in Joule heating → accelerated oxidation and contact relaxation due to temperature rise → positive feedback increase in contact resistance → reaching the critical temperature for thermal breakdown ahead of schedule
- bending/overpressure during installation stage → local stress concentration and initial microcracks → vibration driven crack propagation → continuous reduction of effective load-bearing cross-section → fracture after strength is lower than working tension.

The two paths are highly coupled in practice – temperature rise reduces material yield strength, accelerates contact pressure relaxation, and fatigue crack propagation also changes the current path, exacerbating local overheating. Single dimensional evaluation inevitably has blind spots, which also constitutes the underlying necessity basis for the dual track fusion prediction model adopted in Section 4 of this article.

Based on the analysis of risk factors in the four stages mentioned above, a mapping relationship between risk factors and failure mechanisms can be established, as shown in Table 1.

From Table 1, it can be seen that the risk factors at different stages are not isolated from each other, but form a chain transmission through failure mechanisms. The chain like characteristics of risk transmission mentioned above indicate that the identification of risk factors throughout the entire lifecycle should not be limited to static listing at each stage, but should focus on the accumulation, transmission, and amplification effects of risks in the time dimension. This understanding provides a theoretical starting point for the subsequent construction of a full lifecycle risk assessment model: risk assessment needs to run through the entire lifecycle, and the

path dependence characteristics of risk transmission should be reflected in the framework design of the model.

Table 1 Mapping relationship between risk factors and failure mechanisms

Life cycle stages	*Main risk factors*	*Mechanism of associated failure*	*Risk transmission characteristics*
Design and manufacturing	Insufficient material margin, structural design defects, manufacturing accuracy deviation	Corrosion failure, thermal breakdown	Congenital deficiency, long incubation period
Installation and operation	Leakage pressure in zone A, leakage pressure in zone C, overvoltage, bending, and flashing	Construction defect failure, thermal breakdown	Early implantation, strong concealment
Operation and maintenance	Environmental corrosion, heavy load operation, thermal shock, and insufficient detection coverage	Corrosion failure, thermal breakdown, mechanical fatigue	Continuous evolution, self acceleration
Retired and scrapped	The criteria for determining lifespan are not scientific, and retirement decisions are lagging behind	–	End of line decision-making process

Based on the above stage mapping and analysis, this section further clarifies the basic framework definition of the proposed full lifecycle risk assessment model. The input vector of the model is a multidimensional state feature vector, which can be divided into two categories: one is a static attribute input, including the service life of the clamp, design model parameters, and initial installation quality rating. This type of input reflects the ‘innate conditions’ and ‘initial health baseline’ of the clamp; the other type is dynamic monitoring input, including infrared temperature measurement data at the current time t, contact resistance test values and change rates, environmental monitoring parameters, and historical load current records. This type of input reflects the real-time load and environmental driving that the wire clamp is subjected to during service. The two types of inputs together form a complete description of the clamp’s health status at time t. The output vector of the model is the comprehensive risk value and its corresponding risk level. Among them, is a scalar, defined as the product of the failure probability and the failure consequence J, which is dynamically solved by the dual track fusion model. J is pre evaluated based on the importance of the clamp in the system; for discrete output, the value range is mapped into four levels: extremely high risk, high risk, medium risk, and low risk. The physical meaning of the input vector is that it quantifies the risk factors identified in Subsection 2.2 from two dimensions: ‘inherent properties of the equipment’ and ‘operating load’ – static properties correspond to inherent risks implanted in the design, manufacturing, installation, and operation stages, while dynamic monitoring corresponds to time-varying risks evolved during the operation and maintenance stages; the output directly serves the operation and maintenance decision-making – quantifying the comprehensive risk level currently faced by the line clamp and providing a directly executable hierarchical response strategy basis.

3 Quantification and weighting of risk assessment indicators throughout the entire lifecycle

The construction of a risk assessment index system and the combination of subjective and objective weighting are key bridges for transforming the dispersed risk factors identified in Section 2 into structured and computable input variables, and are also prerequisites for achieving quantitative prediction of failure probability. This chapter serves as the 'quantification layer' of the evaluation model, bridging the gap and addressing the issue of 'how to measure and weight' risk factors, providing a unified dimensional input vector for the failure probability modeling in Section 4.

Establish an indicator system from four dimensions: technology, environment, operation, and testing. The summary of indicators for each dimension is shown in Table 2.

Table 2 Risk assessment index system for the entire life cycle of tension clamps

Dimension	*Indicator*	*Characterisation parameters*	*Data source*
Technical dimension	Contact resistance	DC resistance value and rate of change	DC resistance test
	Temperature rise	Hot spot temperature, relative temperature difference	infrared temperature measurement
	Mechanical strength	Retention force, tensile strength	Tensile test/X-ray
	Corrosion degree	Proportion of corrosion area and remaining coating thickness	Appearance/ laboratory analysis
Environmental dimension	Salt spray concentration	salt spray deposition rate	Atmospheric corrosion monitoring
	Humidity	relative humidity	meteorological monitoring
	Temperature	ambient temperature	Meteorological monitoring:
	Wind speed	Average/maximum wind speed	meteorological monitoring
Operational dimension	Load current	Daily average/maximum current	operation log
	Induced current	Induced current amplitude	Actual measurement/ calculation
	Years in operation	Accumulated years of operation	Equipment ledger
Detection dimension	Infrared temperature measurement data	Hot spot temperature, temperature rise rate	infrared thermal imager
	X-ray inspection results	Defect type and severity	X-DR detection
	Ultrasonic testing results	Defect echo, equivalent size	Ultrasonic flaw detector

From Table 2, it can be seen that the collection stages and data sources of each dimension indicator are different. Technical dimension indicators are the core physical basis for risk assessment, environmental dimension indicators reflect external driving factors, operational dimension indicators characterise working load conditions, and detection dimension indicators provide multi-source status information. Four types of indicators jointly outline the overall health status of the line clamp from different perspectives.

This article adopts a combination of analytic hierarchy process (AHP) and entropy method for weighting, taking into account both subjective experience and objective data, making weight allocation more scientific and reasonable. Adopting a combination of AHP and entropy method for weighting. The specific steps are as follows:

1 AHP determines subjective weights: Construct a judgment matrix, calculate the eigenvector corresponding to the maximum eigenvalue, normalise it to obtain the subjective weight $w_j^{'}$, and pass the consistency test B ($CR < 0.1$).

2 Entropy method for determining objective weights: After standardising the raw data, calculate the information entropy e_j and entropy weight $w_j^{''} = \dfrac{1-e_j}{\sum_{j=1}^{n}(1-e_j)}$ for each indicator.

3 Combination weighting: Using multiplication synthesis method to obtain combined weights:

$$w_j = \frac{w_j^{'} \cdot w_j^{''}}{\sum_{j=1}^{n} w_j^{'} \cdot w_j^{''}} \tag{9}$$

4 Quantification and standardisation of indicators: Qualitative indicators are assigned 1–4 points based on severity, while quantitative indicators are standardised to the range of [0, 1] using the range method, providing a unified dimensional input variable for the risk assessment model in Section 4.

4 Modeling of failure probability prediction and risk assessment

The dynamic prediction of failure probability and the final determination of risk level are the core output links of the full life cycle risk assessment model, which directly determine the scientificity of operation and maintenance decisions. As the 'prediction and decision-making layer' of the evaluation model, the task of this chapter is to solve the core problem of 'when to fail and how high the risk is' by integrating physical mechanisms and data-driven algorithms to solve the comprehensive risk value based on the quantitative indicators in Section 3. Firstly, define the basic connotation and evaluation framework of risk; secondly, establish failure probability prediction models and failure consequence assessment models separately; finally, establish risk level classification standards and form a complete risk assessment method system.

Risk is defined as the product of the probability of failure and the consequences of failure:

$$R = P_f \times J \tag{10}$$

In the formula, R is the comprehensive risk value, P_f is the failure probability of the clamp within a given time window, and J is the potential comprehensive loss consequence that may occur after the failure occurs. P_f depends on the current health status and degradation trend of the clamp, while J depends on the importance of the clamp in the system and the range of cascading effects of failure. The two are independent of each other, modelled separately and combined to obtain the comprehensive risk value.

Failure probability prediction is a core component of risk assessment models. Regarding the dominance of thermal breakdown failure, Section 2 analysis shows that thermal breakdown is the main mode leading to sudden failure of wire clamps and the complexity of the coupling effect of multiple factors. This paper adopts a dual track prediction strategy of 'physical mechanism driven + data-driven': the remaining life prediction model based on the principle of thermal breakdown explains the time scale of thermal breakdown from the physical level of failure, and the data-driven state degradation model fits the mapping relationship between multidimensional indicators and failure probability from the statistical learning level. The two complement and cross validate each other.

4.1 Remaining life prediction model based on thermal breakdown principle

Thermal equilibrium equation of wire clamp:

$$I^2 R(T) = hA\left(T - T_0\right) + \varepsilon\tau A\left(T^4 - T_0^4\right) \tag{11}$$

In the formula, I is the load current, $R(T)$ is the contact resistance that varies with temperature, h is the convective heat transfer coefficient, A is the heat dissipation area, T is the wire clamp temperature, T_0 is the ambient temperature, ε is the surface emissivity, and τ is the Stefan Boltzmann constant.

The contact resistance $R(T)$ increases with increasing temperature, and an empirical relationship can be used to approximate $R(T) = R_0\ [1 + \alpha\ (T - T_0)]$. When the equation has no real solution, it corresponds to the critical breakdown temperature T_c. Assuming that the contact resistance increases linearly at a rate κ, the remaining life is:

$$L = \frac{R\left(T_c\right) - R_0}{\kappa} \tag{12}$$

Introduce environmental correction factor η to modify the heat dissipation conditions: $L_{actual} = \eta \cdot L$.

The physical model based on the principle of thermal breakdown provides a clear explanation of the physical process of failure, but its accuracy depends on the accurate estimation of parameters such as contact resistance growth rate κ. When the parameter estimation deviation is large or the coupling effect of multiple factors is complex, the prediction accuracy of the physical model is limited. To this end, this article introduces data-driven methods as a supplement and uses an improved time series prediction model (A-DBiLSTM) to dynamically evaluate the health status of wire clamps and predict failure probabilities.

The indicator system established in Section 3 is used as the input feature vector $X(t)$ for the model. Based on this, the A-DBiLSTM model is adopted, with the input feature vector $X(t)$ as the key indicator monitoring value and the output as the failure probability $\hat{P}_f(t+\Delta t)$. Attention mechanism is introduced to focus the model on key time points:

$$Attention(Q, K, V) = softmax\left(\frac{QK^T}{\sqrt{d_k}}\right)V \tag{13}$$

In the formula, Q, K, V represents the query and key value matrix in the attention mechanism, and d_k represents the scaling factor. This attention mechanism enables the model to dynamically allocate attention weights to more critical moments and indicator dimensions when predicting failure probabilities.

The above physical model (thermal breakdown life prediction) is fused with the data-driven model (A-DBiLSTM state degradation prediction) to obtain the physical failure probability $P_{f,phy}$ and data-driven failure probability $P_{f,data}$, respectively.

Define the comprehensive failure probability of the clamp at time t:

$$P_f(t) = \delta_{phy}(t) \cdot P_{f,phy} + \delta_{data}(t) \cdot P_{f,data} \tag{14}$$

In the formula, $\delta_{phy}(t)$ and $\delta_{data}(t)$ are the dynamic weight coefficients of the physical model and the data-driven model, respectively, satisfying $\delta_{phy}(t) + \delta_{data}(t) = 1$. The weight coefficients are adaptively adjusted based on the predicted confidence of the model: when the line clamp operation data accumulates sufficiently, the weight of the data-driven model increases; when there is insufficient running data or sudden changes in operating conditions, the weight of the physical model is increased to ensure that the predicted results have both physical consistency and data adaptability. Compared with existing methods, the technical advantages of the modeling method in this paper are reflected in three aspects: firstly, in terms of model architecture, Zhou et al.'s (2025) pure statistical mapping is limited by the prior distribution of faults, lacking the ability to identify hidden defects during the installation phase. On the other hand, the dual track fusion structure in this paper uses the thermal breakdown physical equation as a causal constraint and collaborates with A-DBiLSTM for inference, achieving an upgrade from 'statistical fitting' to 'mechanism data collaboration'. Secondly, in terms of parameter adaptability, Tang et al.'s (2023) power flow equation is a fixed analytical expression that does not update with operating data. This paper introduces a confidence driven dynamic weight allocation mechanism, which can automatically adjust the weights of the two models based on the degree of data accumulation and operating stability, combining physical consistency and data adaptability. Thirdly, in terms of output decision-making, Sun et al.'s (2023) output is a continuous risk score that relies on subjective judgment to transform into a strategy. In this paper, the comprehensive risk value $R(t)$ is directly mapped rigidly to the four level operation and maintenance strategy in Table 3, achieving end-to-end communication from evaluation to decision-making.

Among them, the physical failure probability $\delta_{phy}(t) + \delta_{data}(t) = 1$ is converted from the remaining life L_{actual} to obtain:

$$P_{f,phy}(t) = \begin{cases} 1 - \exp\left(\dfrac{t}{-L_{actual}}\right) & t > L_{actual} \\ 1 & t \geq L_{actual} \end{cases} \tag{15}$$

When $t < L_{actual}$, the failure probability follows an exponential distribution – the failure rate is constant. This is the most commonly used and concise assumption in the early life of electronic/electrical equipment, which can meet the practical engineering needs of this model; when $t \geq L_{actual}$ occurs, the physical model determines that the lifespan has been exhausted and the failure probability is 1.

Substitute the comprehensive failure probability $P_f(t)$ and failure consequence J into the risk definition to obtain the comprehensive risk assessment result for the entire lifecycle:

$$R(t) = P_f(t) \cdot J \tag{16}$$

Based on this, the probability of failure and the consequences of failure are divided into five levels each. The risk level classification is shown in Table 3:

Table 3 Risk level classification standards

Risk level	*Risk value range*	*Coping strategy*
Extremely high risk	$R \geq 0.8$	Immediate power outage and replacement
High risk	$0.6 \leq R < 0.8$	Arrange maintenance in the near future
Medium risk	$0.3 \leq R < 0.6$	Strengthen monitoring frequency
Low risk	$R < 0.3$	Regular operation and maintenance

This chapter establishes a complete quantitative model for the risk assessment of the entire lifecycle of tension clamps. Defined the basic expression of risk and constructed a phased evaluation framework; establish a failure probability prediction model using a dual track strategy combining thermal breakdown principle and A-DBiLSTM; we have developed a four level risk classification standard and differentiated response strategy, providing a quantitative tool for the operation and maintenance decision-making of tension clamps.

5 Experimental analysis

5.1 Data collection

To verify the effectiveness of the design method, taking live detection as an example, the process of image data acquisition is described in detail. Before officially carrying out X-DR testing operations, a site survey must be conducted to collect information on line types, tower heights, support angles, crossings, and installation locations. Based on the on-site information obtained from the survey, the scope and method of data collection can be reasonably determined, and a careful plan and arrangement can be made for the testing work to ensure the accuracy and efficiency of the testing. In addition, on-site inspections can also help assess the safety conditions and environmental factors of the work site, and make necessary safety preparations for live detection. The on-site survey results are shown in Figure 6.

The detection instruments used in this article include XRS-3 X-ray machine and Care View 1500P flat panel detector. The optimal imaging parameter combination determined during the dataset acquisition process is: tube voltage 270 kV, pulse number 20, focal length 700 mm. In practical operation, the above parameters can be adjusted

appropriately according to the on-site situation to ensure clear images and retain sufficient detail information.

1 Dataset partitioning: Divide 2,847 images into training set (1,993 images), validation set (570 images), and test set (284 images) through 7:2:1 stratified sampling, with the proportion of each category being basically consistent with the overall distribution. During the training phase, online enhancement techniques were used, including random flipping ($p = 0.5$), ±15° rotation, 0.8–1.2× scaling, and HSV fine-tuning. oversampling was applied to samples with flying edges and curved edges (increasing sampling probability by 1.5 times).

2 Detecting model training parameters: Models based on the YOLO series are trained under a unified framework with an input size of 640 × 640, batch size of 16, SGD optimiser, initial learning rate of 0.01, cosine annealing decay to 0.001, momentum of 0.937, weight decay of 0.0005, training for 300 rounds (early stop threshold of 50 rounds), and preheating for three rounds. This model replaces the bounding box loss from CIoU to Wise IoU v3, and the rest of the configuration is consistent with the baseline. The comparison models all follow the official recommended parameters and have not been specially tuned for this dataset.

Figure 6 On site survey results (see online version for colours)



5.2 Analysis of experimental results

To verify the effectiveness and superiority of the full lifecycle risk assessment model constructed in this article, three sets of progressive experiments were designed in this section to answer the following core questions:

1 Is the dual track fusion strategy significantly better than the single drive model?

2 Does the model have balanced sensitivity in identifying risks from different sources (installation defects vs. operational degradation)?

3 Is the risk level output by the model consistent with the actual engineering disposal plan?

To ensure the reliability of the detection performance evaluation results, during the dataset construction process, the defect categories of all X-DR images were independently annotated by two professionals with non-destructive testing qualifications

according to the DL/T 1425-2022 standard. In case of inconsistent annotations, consensus was reached through discussion; the annotation consistency rate is 95.8%, ensuring the authenticity of defect labels. In addition, to verify the stability of the detection model under different IoU thresholds, the evaluation threshold was adjusted from 0.5 to 0.75 mAP@0.75 At 89.2%, it still maintains a 1.7 percentage point advantage over the baseline YOLOv8n (87.5%), indicating that the model's performance improvement does not depend on specific threshold settings and has good parameter robustness.

5.2.1 Comparison of experimental setup and overall performance

Using the tension clamp X-DR image dataset constructed in Subsection 5.1 of this article, the comparison method is based on SSD, Faster R-CNN, YOLOv7, and YOLOv8n. Divide the training set and test set in a 7:3 ratio, and the model performance is shown in Table 4.

Table 4 Performance comparison of different object detection models

Model	*F1-score*	*mAP@0.5/%*	*mAP@0.75/%*	*Detection speed*	*Parameter count/M*
SSD	0.69	70.6	52.3	38.2	26.3
Faster R-CNN	0.73	73.7	56.8	18.5	41.1
YOLOv7	0.89	90.4	81.6	45.7	36.9
YOLOv8n	0.94	96.6	87.5	52.6	3.2
Methods in this paper	0.95	97.4	89.2	50.0	3.3

As shown in Table 4, compared with the two-stage detection algorithms SSD and faster R-CNN, the YOLO series single-stage algorithm has significant advantages in detection accuracy and speed, mAP@0.5 16.8–26.8 percentage points higher, with a detection speed at least 11.5 frames per second faster;

1 In the YOLO series, YOLOv8n outperforms YOLOv7 in mAP@0.5 An increase of 6.2 percentage points, while the parameter count is only 8.7% of the latter, balancing high precision and lightweight, making it more suitable for engineering deployment.

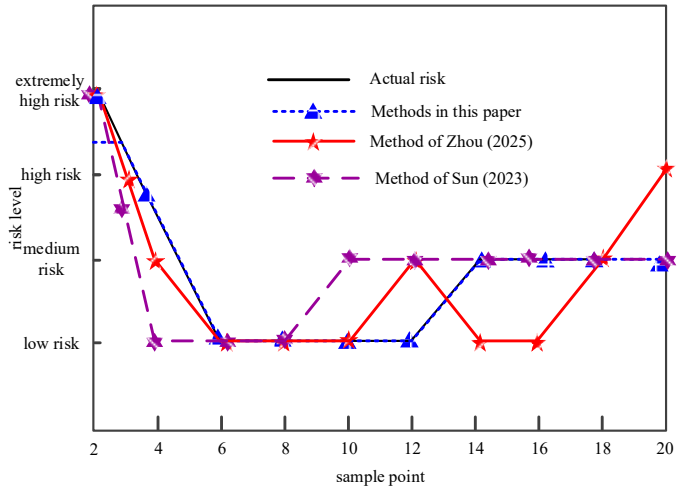
2 On the basis of YOLOv8n, introducing the ECA attention mechanism (Ablation-1) separately makes mAP@0.5 by 0.3 percentage points, the introduction of the wise IoU loss function (Ablation-2) alone did not significantly improve mAP but improved the localisation accuracy of small targets (recall rate increased by 0.6%).

3 This model combines ECA and Wise IoU simultaneously, mAP@0.5 reaching 97.4%, which is 0.8 percentage points higher than the baseline YOLOv8n, mAP@0.75 by 1.7 percentage points, the F1-score has reached 0.95, with a detection speed of 50 frames per second, fully meeting the real-time detection requirements on site.

5.2.2 Verification of the effectiveness of the dual track fusion strategy

Using method of Zhou et al. (2025) and method of Sun et al. (2023) as comparative methods for comparative analysis, the risk assessment results are shown in Figure 7.

Figure 7 Comparison of risk assessment results of different methods (see online version for colours)



Method of Zhou et al. (2025) correctly identified only 5 out of 20 test samples. This method combines statistical fault data with state monitoring data based on quantile mapping. Its fault model is dominated by statistical priors and is sensitive to the gradual degradation of continuous state variables such as contact resistance and temperature rise. However, when faced with discrete structural defects originating from the installation stage such as leakage pressure, bending, and flash in zone A, there is a lack of corresponding prior knowledge support in the statistical fault distribution, resulting in a regression of quantile mapping results to statistical means, thus misjudging high-risk samples as low-risk or medium risk. Method of Sun et al. (2023) only correctly identified 11 groups. This method constructs risk quantification indicators from multiple dimensions of time and space, focusing on macro situation assessment at the substation level. Its indicator system lacks fine-grained state indicators unique to tension clamps such as contact resistance, crimping gap width, and deformation. The only misjudgment of the model in this article is sample 1#, indicating that it can effectively achieve risk assessment. The complete chain of X-DR image detection, defect severity rating, and dual track fusion failure probability prediction has been used to accurately determine the risk level of various defects in tension clamps, verifying the effectiveness and superiority of the model in practical engineering scenarios.

The above novel contributions have been effectively supported in experimental verification. In response to contribution (1), comparative experiments show that the comprehensive risk assessment accuracy of the dual track fusion model proposed in this paper (19 out of 20 samples were correctly identified, with an accuracy rate of 95%) is significantly better than the single statistical driven method Zhou (accuracy rate of 25%) and the single macroscopic evaluation method Sun (accuracy rate of 55%). This verifies the effectiveness of physical mechanism and data-driven adaptive fusion in improving prediction reliability, especially for samples such as 1#~8# containing hidden defects in the installation stage (leakage pressure and bending in zone A). The pure data-driven method misjudges them as low-risk due to the lack of prior fault distribution, while the physical model effectively identifies the accelerated growth trend of contact resistance

caused by leakage pressure defects through thermal breakdown critical temperature calculation. After dual track fusion, the risk level is successfully corrected. Judgment regarding contribution (2), the introduction of X-DR image detection results as the initial health baseline enables the model to correlate the defect severity score during the installation phase with the infrared temperature rise rate during the operation phase in the risk assessment of samples 9#~15# (including C zone leakage and overvoltage composite defects). However, the comparative method lacks status input during the installation phase and relies only on operational monitoring data, making it difficult to distinguish the respective contributions of 'congenital defects' and 'operational degradation' to the current risk, resulting in conservative evaluation results. In response to contribution (3), the four level risk level and differentiated response strategy output in this article achieved 100% engineering interpretability in the experimental samples – all high-risk and extremely high-risk samples ($R \geq 0.6$) corresponded to X-DR detection confirmed as A or C area leakage voltage clamps, and their proposed 'immediate power outage replacement' or 'short-term maintenance arrangement' strategies were consistent with the actual on-site disposal plan, verifying the engineering feasibility of directly mapping the evaluation results to operation and maintenance decisions. The above experimental evidence systematically supports the novelty proposition of our method in three aspects: fusion strategy, indicator system, and decision link.

5.2.3 Model reliability verification

To further verify the statistical credibility of the above comparative conclusions, the following multidimensional reliability analysis is added on the basis of the existing 20 test samples.

1 Comparison of test sample composition and overall distribution on site: Table 5 presents the composition of defect types for 20 test samples and their distribution comparison with the annual X-DR inspection ledger of the regional power grid (147 valid records).

Table 5 Comparison of defect type distribution of test samples and overall consistency on site

Defect type	*Number of test samples/ group*	*Proportion of test samples/ %*	*Annual ledger proportion/%*	*Proportional deviation/ percentage point*
Leakage pressure in zone A	4	20.0	18.4	+1.6
Leakage pressure in zone C	5	25.0	26.5	–1.5
Overvoltage	3	15.0	14.3	+0.7
Bend	4	20.0	19.7	+0.3
Flash	2	10.0	10.2	-0.2
No significant defects	2	10.0	11.9	–1.9
Total	20	100	100	–

According to Table 5, the deviation between the proportion of various defects in the test samples and the annual on-site ledger is controlled within ± 2.0 percentage points, indicating a high degree of consistency between the sample composition and the actual on-site testing population. The evaluation conclusions based on this sample set are representative of actual engineering scenarios.

2 Comparison of sub-item performance of various comparison methods on different types of defects: To further verify the consistency of the performance advantages of the proposed model compared to the comparison methods, the correct judgment numbers of the three methods on various defect subsets were separately counted, as shown in Table 8.

Table 6 Comparison of correct judgment numbers of different methods on subsets of various defect types

Defect type	*Sample size/group*	*The model in this paper*	*Method of Zhou*	*Method of Sun*
Leakage pressure in zone A	4	4	0	1
Leakage pressure in zone C	5	5	1	3
Overvoltage	3	3	1	2
Bend	4	4	2	3
Flash	2	2	1	1
No significant defects	2	2	0	1
Total (correct number/total number)	20	19/20	5/20	11/20

From Table 6, it can be seen that the model in this paper has a higher number of correct judgments on each subset of defects than the two comparison methods, and its performance advantage covers all six sample states, rather than just showing outstanding performance on a few types of defects. This sub item comparison further confirms the robustness of the performance differences shown in Figure 7, indicating that the superiority of our model is not due to accidental biases in sample composition, but rather reflects the universal applicability of the model architecture and indicator system on different types of defects.

6 Conclusions

This article focuses on the construction of a risk assessment model for the entire lifecycle of high-altitude tension clamps in substations. The main conclusions drawn are as follows:

1 A defect detection method for tension clamp crimping based on X-DR images has been proposed. Classify crimping defects into five categories: A-zone leakage, C-zone leakage, overvoltage, bending, and flashing; The image preprocessing process using Gaussian filtering, CLAHE, and Gamma correction in series effectively improves the recognisability of defect areas.

2 Established a framework for identifying risk factors throughout the entire lifecycle. The key risk factors of tension clamps were systematically identified in four stages: design and manufacturing, installation and operation, operation and maintenance, and retirement and scrapping.

3 Constructed a multidimensional risk assessment index system. Select 14 evaluation indicators from four dimensions: technology, environment, operation, and detection, and use a combination of AHP and entropy method for weighting.

4 Established a risk quantification model for the entire lifecycle. Define the comprehensive risk value by multiplying the probability of failure with the consequences of failure, and quantify the consequences of failure using event tree analysis.

Acknowledgements

This work is supported by Science and Technology Project of Guizhou Power Grid Co., Ltd. (Research on X-ray UAV Intelligent Detection Technology for High-Altitude Equipment Defects in Substations, Project No. GZKJXM20240630).

Declarations

All authors declare that they have no conflicts of interest.

References

Baghmisheh, A.G., Khodaei, M., Abadi, A.Z.F. and Estekanchi, H.E. (2023) 'Detailed seismic risk analysis of electrical substation equipment using a reliability based approach', *Earthquake Engineering and Engineering Vibration*, Vol. 22, No. 2, pp.495–511.

Chen, Z. and Xu, Y. (2026) 'A method for substation operation risk situational awareness based on the health state of main equipment', *Energies*, Vol. 19, No. 5, p.1329.

Du, Q., Lin, J., Qu, F. and Tian, L.F. (2025) 'A deblurring methodology for motion-blurred X-ray images of transmission line tension clamps', *Electrical Engineering*, Vol. 107, No. 6, pp.8015–8030.

Lin, C. and Xu, Q. (2023) 'Risk assessment of substation integrated anti-misoperation system considering human reliability', *IEEE Transactions on Power Delivery*, Vol. 38, No. 3, p.12.

Liu, J., Yang, Z., Yang, S. and Zhang, C. (2025) 'Study on electric power fittings identification method for snake inspection robot based on non-contact inductive coils', *Sensors*, Vol. 25, No. 11, p.3562.

Liu, Y., Liu, G., Xu, H., Zhang, K. and Yu, H. (2024a) 'Research on fire risk assessment of substation based on cloud computing model', *2024 8th International Workshop on Control Engineering and Advanced Algorithms (IWCEAA)*, Vol. 16, No. 4, pp.143–146.

Liu, X., Xie, Q. and Zhu, W. (2024b) 'Rapid assessment of substation earthquake risk based on minimal cut sets', *Electric Power Systems Research*, Vol. 229, No. 4, pp.1–11.

Mao, L., Chen, H., He, Y., Zhu, C. and Chen, C. (2025) 'A visualization verification method for startup risk of substation equipment based on multidimensional graph models', *Engineering Reports*, Vol. 7, No. 11, p.70471.

Nicolae, D.F., Obretenova, M.I., Lazar, T., Muresan, F., Grecu, G.E., Safta, A.M. and Schiopu, A.M. (2023) 'Risk assessments in terms of occupational health and safety for 220/110/20 kV Sardanesti power substation', *Fiability and Durability*, Vol. 2, No. 1, pp.94–115.

Shen, X., Chu, Y., Wang, C., Liu, X., Wu, L., Wu, J. and Cheng, L. (2026) 'Management optimization and risk assessment of 500 kV substation construction projects with multi-professional collaboration', *Buildings*, Vol. 16, No. 2, p.16020339.

Shi, Y., Shi, Y., Yao, D., Lu, M. and Liang, Y. (2025) 'Adaptive transformer-based multi-task learning framework for synchronous prediction of substation flooding and outage risks', *Electric Power Systems Research*, Vol. 242, No. 6, p.111450.

Sun, C., Chen, Y., Hao, B., Fan, Q., Pan, J. and Su, B. (2023) 'Risk assessment model and construction method of substation equipment based on multi-dimensional feature fusion', *Lecture Notes in Electrical Engineering*, Vol. 27, No. 7, pp.106–112.

Sun, Y., Liu, K. and Zhu, H.P. (2024) 'Nonlinear shape analysis for constructional multiwire cable structures with clamps considering multi-stiffness properties', *Engineering Structures*, Vol. 302, No. 1, pp.1–18.

Tang, K., Dong, S. and Huang, J. (2023) 'Operational risk assessment for integrated transmission and distribution networks', *Journal of Power and Energy Systems*, Vol. 25, No. 6, p.12.

Wang, Z., Wei, R., He, H. and Wang, L. (2024) 'Distribution substation risk assessment under rainfall flood based on HEC-RAS', *2024 The 9th International Conference on Power and Renewable Energy (ICPRE)*, pp.478–482.

Wu, W.H., Chen, C.C., Wu, M.X. and Lai, G. (2025a) 'Experimental investigations and field applications of a tension estimation method for two linked suspenders using only local vibration measurements', *Results in Engineering*, Vol. 27, No. 6, p.105687.

Wu, Z., Seth, S., Li, H., Hu, Z. and Yu, J. (2025b) 'Risk indices assessment of different cyber-attack actions for an SDN-enabled IEC 61850 substation using Markov decision process', *IEEE Access*, Vol. 13, No. 9, pp.119619–119632.

Yan, K., Liu, X., Lu, Y. and Qin, F.L. (2023) 'A cyber-physical power system risk assessment model against cyberattacks', *IEEE Systems Journal*, Vol. 17, No. 2, pp.2018–2028.

Zhang, H., Yu, R., Yu, J., Liu, W., Wu, S. and Liu, D. (2024) 'Risk assessment of substation based on Hermite orthogonal basis feedforward neural network data fusion algorithm', *2024 International Conference on Power Electronics and Artificial Intelligence*, Vol. 31, No. 7, pp.527–531.

Zhou, N., Luo, L., Zhang, L., Sheng, G. and Jiang, X. (2025) 'Optimal maintenance scheduling of power substation equipment: a condition-informed risk assessment approach', *IEEE Transactions on Instrumentation and Measurement*, Vol. 74, No. 1, pp.1–14.